Journal of Physics D: Applied Physics

PAPER

The study of interface quality in HfO_2/Si films probed by second harmonic generation

To cite this article: Li Ye *et al* 2024 *J. Phys. D: Appl. Phys.* **57** 415105

IOP Publishing Journal of Physics D: Applied Physics
J. Phys. D: Appl. Phys. **57** (2024) 415105 (9pp) https://doi.org/10.1088/1361-6463/ad61f9

The study of interface quality in HfO_2/Si films probed by second harmonic generation

Li Ye[1,2,8], Libo Zhang[1,2,8], Shaotong Wang[3], Weiwei Zhao[3], Chongji Huang[3], Wenshuai Gao[1], Xue Liu[1], Tiaoyang Li[4], Tao Li[5], Tai Min[5], Mingliang Tian[6] and Xuegang Chen[1,7,*]

[1] Center of Free Electron Laser & High Magnetic Field, Leibniz International Joint Research Center of Materials Sciences of Anhui Province, Hefei 230601, People's Republic of China
[2] School of Materials Science and Engineering, Anhui University, Hefei 230601, People's Republic of China
[3] Shanghai Aspiring Semiconductor Equipment Co., Ltd & Aspiring Semiconductor (Beijing) Co., Ltd, Shanghai 200082, People's Republic of China
[4] College of Physics and Information Engineering, Fuzhou University, Fuzhou 350108, People's Republic of China
[5] Center for Spintronics and Quantum Systems, State Key Laboratory for Mechanical Behavior of Materials, Department of Materials Science and Engineering, Xi'an Jiaotong University, Xi'an, Shaanxi 710049, People's Republic of China
[6] School of Physics and Optoelectronic Engineering, Anhui University, Hefei 230601, People's Republic of China
[7] Information Materials and Intelligent Sensing Laboratory of Anhui Province, Anhui Key Laboratory of Magnetic Functional Materials and Devices, Anhui University, Hefei 230601, People's Republic of China

E-mail: xgchen@ahu.edu.cn

Received 17 April 2024, revised 19 June 2024
Accepted for publication 11 July 2024
Published 22 July 2024

Abstract

Time-dependent second harmonic generation (TD-SHG) is an emergent sensitive and non-contact method to qualitatively/quantitively characterize the semiconductor materials, which is closely related to the interfacial electric field. Here, the TD-SHG technique is used to study the interface quality of atomic layer deposited 15 nm HfO_2/Si (*n*-type/*p*-type) samples, which is compared to the conventional electrical characterization method. A relation between the interface state density and the time constant extracted from TD-SHG is revealed, indicating that TD-SHG is an effective method to evaluate the interface state density. In addition, the dopant type and dopant density can be disclosed by resolving the dynamic process of TD-SHG. The scenario of interfacial electric field between the initial electric field and the laser-induced electric field is proposed to explain the time-dependent evolution of SHG signal. In conclusion, the TD-SHG is a sensitive and non-contact method as well as simple and fast to characterize the semiconductor materials, which may facilitate the semiconductor in-line testing.

Keywords: time-dependent second harmonic generation, interface state density, dopant type/density, high k material

[8] These authors contribute equally to the work.
[*] Author to whom any correspondence should be addressed.

1. Introduction

To accommodate the miniaturization of field-effect transistors (FETs), the high-k gate oxides have been developed recently, including hafnium oxide (HfO_2), zirconium oxide (ZrO_2), and alumina (Al_2O_3) [1, 2]. Among the potential candidates, HfO_2 becomes a leading material due to its superior high-k gate dielectric characteristics. It persists a relatively large band gap (>5 eV) [3], a high dielectric constant (∼25) [4], the good thermal and thermodynamic stability in contact with silicon [5]. Consequently, HfO_2 has been the focus of extensive research, especially for its application in high-k gate dielectrics as FETs [6, 7].

The high-k materials under consideration are prone to intrinsic and process-induced defects, which can trap electrons through the localized states. Therefore, it can affect the device performance. These defects in the gate dielectric films can lead to various issues, including increased leakage current, lowered breakdown voltage, threshold voltage instability and decreased carrier mobility/lifetime [8]. A high-quality oxide-semiconductor interface with a low interface state density is crucial for semiconductor applications. Therefore, a precise characterization of defects and interface state density is essential for advancing the performance and reliability of semiconductor devices.

Traditionally, electrical methods such as the capacitance–voltage (C–V) method or conductance method have been employed to characterize the electroactive defects in the silicon-oxide systems [9, 10]. However, these methods come with notable limitations. The electrical methods need to fabricate the well-constructed electrode contacts which tends to be destructive as well as a time-consuming process. The tested samples cannot be further processed in the device fabrication sequence, namely the electrical methods cannot be directly incorporated into the device fabrication sequence. Consequently, there's an urgent need for fast, non-destructive characterization techniques that can accurately measure electroactive defects and be smoothly integrated into the manufacturing workflow. The optical methods offer the promising alternatives for efficient, non-destructive, non-contact characterization of defects, which may facilitate the semiconductor device manufacture.

Optical second harmonic generation (SHG) is a nonlinear optical phenomenon that serves as a sensitive probe for studying buried solids and interfacial properties [11]. The sensitivity of SHG to interfacial electrical properties, such as charge traps [12] and doping levels [13, 14], makes it as a unique characterization technique. In the centrosymmetric materials, dipole contributions at the lowest order are typically prohibited, except the dipole contribution at the interface where inversion symmetry is disrupted due to material discontinuity as well as the interfacial electric field. This inversion symmetry breaking could generate the SHG signal. The SHG intensity ($I_{2\omega}$) can be expressed as [15]:

$$I_{2\omega}(t) \propto \left|\chi^{(2)}_{\text{interface}} + \chi^{(3)}\left[E_0 + E(t)\right]\right|^2 (I^{\omega})^2 \qquad (1)$$

where $\chi^{(2)}_{\text{interface}}$ and $\chi^{(3)}$ are the second-order and third-order nonlinear susceptibility tensors, respectively. E_0 is the initial static built-in electric field while I^{ω} is the intensity of the incident laser. The term of $\chi^{(3)}E_0$ describes the electric field induced second harmonic effect, which has proven to be a very sensitive probe for internal electric fields. At the dielectric/semiconductor interface, an additional electric field $E(t)$ could be generated by the laser illuminated on the sample, which also varies with the time of illumination. The time dependent evolution of SHG is closely related to the trapping and detrapping process of laser excited electrons in the dielectric/semiconductor system [16].

Various studies have verified that the SHG technique is an efficient characterization of silicon-based dielectrics (SiO_2 and high-k materials), offering profound insights into the interfacial properties of silicon-based oxides. Fomenko *et al* explored the uniformity in the distribution of interfacial defects across gate dielectric films such as SiO_2, Al_2O_3, ZrO_2, and HfO_2 on Si. They employed the rotational anisotropy SHG to assess the optical roughness of the films, which is regarded as a quantity describing the nonuniformity in the distribution of interfacial defects [17]. In another study, the detailed characterizations of interface state density at the HfO_2/Si film were conducted by the SHG technique. These qualitative/quantitative evaluations provide the details about energy band bending at the HfO_2/Si interface [18]. Therefore, the TD-SHG should be a promising method to efficiently characterize the defects and interface state density in the dielectric/semiconductor structures.

In this work, the HfO_2 thin films on *n*-type and *p*-type Si substrate were grown by the atomic layer deposition. The conductance method ($G/\omega - V$ measurement) is used to extract the interface state density of the Au/HfO_2/Si structure. A correlation between SHG intensity and interface state density is established to evaluate the quality of the HfO_2 films. We also reported the measurement that a two-photon absorption is required to promote electrons from the valence band of Si to the conduction band of HfO_2 at an incident photon energy of 1.59 eV via multiphoton internal-photoemission induced second-harmonic generation technique. At last, we investigated the TD-SHG for the *n*-doped and *p*-doped HfO_2/Si systems at various doping concentrations. Our findings indicate that the SHG signal exhibits sensitivity to the dopant type and concentration. We attribute these observations to the electric field formed by the initial electric field and the laser-induced electric field, which ultimately drive electric field induced SHG and influence the resulting SHG curves. Our study indicates that the optical SHG is a highly efficient and non-destructive method to characterize the semiconductor materials, which provides a simple and fast solution for in-line testing.

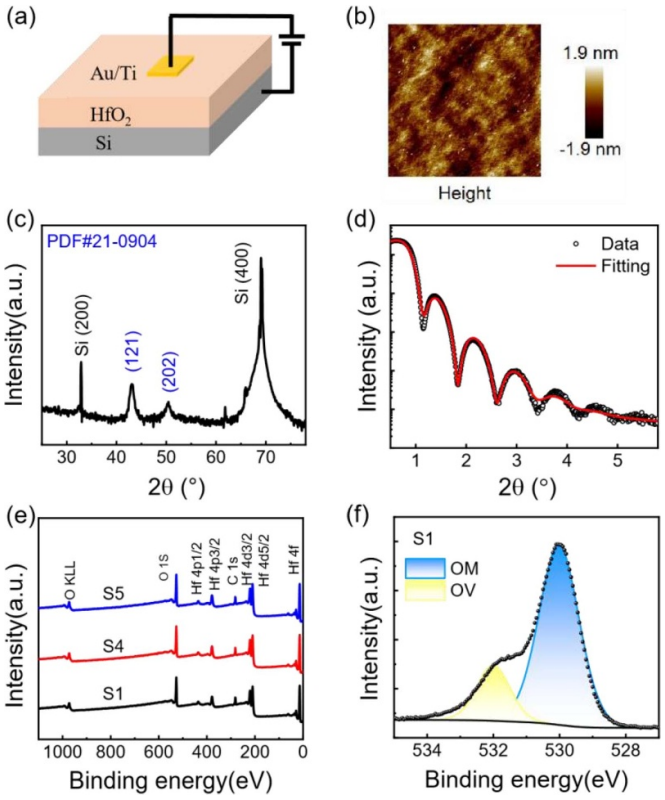

Figure 1. (a) The measurement schematic of Au/HfO_2/Si structure. The positive voltage is defined as a voltage applied on the Au electrode. The area of Au electrode is 50 μm × 50 μm. (b) The typical AFM image of as-deposited HfO_2 film with a scanning area of 4 μm × 4 μm. (c) The typical x-ray diffraction (XRD) pattern and (d) The x-ray reflectivity (XRR) pattern and the fitting of as-deposited HfO_2 film. (e) The x-ray photoelectron spectroscopy (XPS) of S1, S4, S5 samples. (f) The fitting of XPS data for S1 sample.

2. Experiments

The HfO_2 films (15 nm) were deposited on Si substrates via the atomic layer deposition. The samples are classified by dopant density of *n*-type Si substrate (S1: $\sim 8 \times 10^{13}$ cm^{-3}, S2: $2 \times 10^{17} - 5 \times 10^{18}$ cm^{-3}, S3: $\geqslant \sim 8 \times 10^{19}$ cm^{-3}) and *p*-type Si substrate (S4: $\sim 2 \times 10^{12}$ cm^{-3}, S5: $\sim 2 \times 10^{14}$ cm^{-3}, S6: $7.5 \times 10^{17} - 8.5 \times 10^{18}$ cm^{-3}). The squared metal electrodes (Au (50 nm)/Ti (5 nm)) were fabricated using the conventional photolithography and followed by the electron beam evaporation (shown in figure 1(a)). The surface morphology of the HfO_2 films was examined by the atomic force microscopy (AFM, model AFM5500M). The crystalline structure of HfO_2 thin films was investigated by the x-ray diffraction (XRD, model D8 ADVANCE), while the x-ray reflectivity (XRR) was employed to estimate the film thickness. X-ray photoelectron spectroscopy (XPS, model AXIS, SUPRA+) was applied to study the valence state and oxygen state in the films. The capacitance–voltage (C–V) and conductance–voltage (G/ω–V) measurements were conducted using a Keysight E4980A precision LCR meter and the data collection was facilitated by a custom Labview program. The TD-SHG measurements were conducted by Aspirer 3000 system using a pulsed laser with wavelength of 780 nm, pulse duration of 150 fs, and repetition frequency of 70 MHz. The laser beam was focused on the sample at 45°. The *p*-polarized SHG signal ($\lambda = 390$ nm) was collected under the excitation of *p*-polarized fundamental radiation ($\lambda = 780$ nm). The spot area is 7×10^{-6} cm^2. The average power intensity and the peak power intensity irradiation on the samples are 42.4 kW cm^{-2} and 4.1 GW cm^{-2} respectively. P-polarized photons were detected by photomultiplier, whereas the samples were placed in the air. The TD-SHG experiments were performed with a specific azimuthal angle, which is determined by rotation-anisotropy SHG results to provide a standard process of charge evolution.

3. Results and discussion

Figure 1(b) displays a typical AFM image of the as-deposited HfO_2 thin film with a surface roughness of 0.44 nm, indicating a flat surface of HfO_2 film. Figure 1(c) presents the XRD pattern of the HfO_2 film on a Si substrate. Clear diffraction peaks from HfO_2 locating at 43.2° (121) and 50.4° (202) is observed (Ref: No.21-0904). No impurity peak is identified. The thickness of HfO_2 is calculated to be ∼15 nm based on the x-ray reflectivity (figure 1(d)), which also verifies the flat surface of as-deposited HfO_2 film. Figure 1(e) shows the XPS spectra for three as-deposited HfO_2 films in a wide range, which is calibrated by the C 1s peak at 284.8 eV. The spectra reveals the presence of Hf and O, which is consistent with previous results [19]. To deduce the oxygen vacancy concentration in the HfO_2 films, the O 1s spectra is deconvoluted from the XPS spectra. The typical deconvolution data is displayed in figure 1(f). Here, oxygen molecule (OM) represents the bonded state of oxygen in the oxide lattices without vacancies correlating to the peak at 530 eV while oxygen vacancy (OV) denotes the bonded state of OVs related to the hydroxyl groups (shown as the shoulder near the OM peak) [20]. The estimated peak intensity ratios (I_0) between the low-energy satellite peak near 532 eV and the total oxygen peak intensity are 20.39%, 12.22%, and 16.69% for the S1, S4, and S5 samples, respectively. Given that an OV releases two electrons and two molecular units per unit cell, the OV concentration can be estimated as $1/4 \times I_0$. Accordingly, the OV concentration of S1, S4, and S5 films can be estimated to be 5.10%, 3.05%, and 4.17%, respectively, which is slightly larger compared to previous reports [21].

The corrected capacitance–voltage (C–V) characteristics of Au/HfO_2/Si structure (*n*-type Si and *p*-type Si) under various frequencies (1–500 kHz) are displayed in figures 2(a) and (c). For the Au/HfO_2/Si (*n*-type) sample, the three regimes of accumulation, depletion and inversion are clearly shown in figure 2(a), verifying a typical MOS behavior with conventional C–V characteristics [22, 23]. At a large negative voltage, the capacitance curve at the high frequency (500 kHz) is independent of gate bias. The upturn of capacitance with decreasing frequency at negative bias is likely due to the

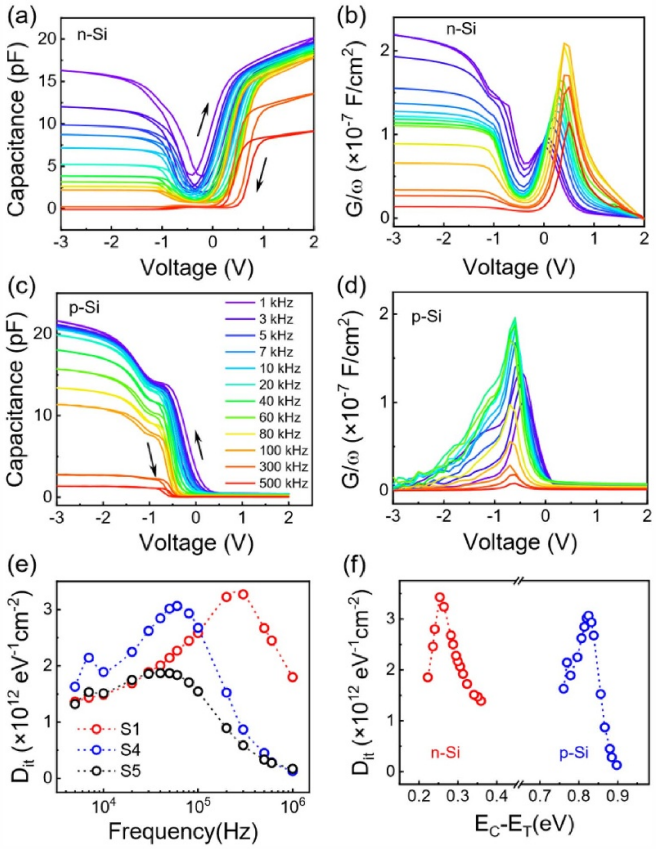

Figure 2. The corrected C–V and G/ω characteristics for Au/HfO_2/Si sample with *n*-type Si substrate (a) and (b) (S1 sample) and with *p*-type Si substrate (c) and (d) (S4 sample). (e) The calculated D_{it} versus frequency (semilog) for S1, S4, S5 samples. (f) The distribution of calculated D_{it} for S1 sample (*n*-type) and S4 sample (*p*-type).

response of interface trap. A clear frequency dispersion at the accumulation region (+2 V) is observed in the Au/HfO_2/Si (*n*-type) sample, especially at high frequency region, which is closely related to the border traps near the interface or series resistance in the MOS structure (figure 2(a)) [24, 25]. It also contributes to the observed C–V hysteresis. In addition, a shift of flat-band voltage ($\Delta V_{fb} = 0.27$ V at 500 kHz) is revealed, which is consistent with previous reports [26, 27]. As for the Au/HfO_2/Si (*p*-type) sample, no frequency dispersion is displayed at the depletion/inversion region (positive bias). The shift of flat-band voltage is −0.15 V at the frequency of 500 kHz.

Here, we used the conductance method to extract the density of interface state. Firstly, Nicollian and Goetzberger method is used to extract the series resistance [28, 29]. The strong accumulation admittance (Y_{ma}) of MOS capacitor could be calculated from the equation (2) including the measured capacitance (C_{ma}), and conductance (G_{ma}) (in strong accumulation):

$$Y_{\mathrm{ma}} = G_{\mathrm{ma}} + j\omega C_{\mathrm{ma}}. \tag{2}$$

Accordingly, the series resistance is the real part of the impedance ($Z_m = 1/Y_m$), which is given by the relation:

$$R_s = \frac{G_{\mathrm{ma}}}{(G_{\mathrm{ma}})^2 + (\omega C_{\mathrm{ma}})^2} \tag{3}$$

where ω is the angular frequency ($\omega = 2\pi f$, f: frequency). The calculated Rs values are used to correct the capacitance and conductance. The corrected C–V and $G/\omega - \mathrm{V}$ curves were obtained by using the following relations:

$$C = \frac{\left[(G_m)^2 + (\omega C_m)^2\right] C_m}{a^2 + (\omega C_m)^2} \tag{4}$$

$$G = \frac{\left[(G_m)^2 + (\omega C_m)^2\right] a}{a^2 + (\omega C_m)^2} \tag{5}$$

where $a = (G_m) - [(G_m)^2 + (\omega C_m)^2]R_s, C_m$ is the measured capacitance and G_m is the measured conductance. The corrected G/ω-V characteristics for the Au/HfO_2/Si structure are illustrated in figures 2(b) and (d). Clearly, the value of G/ω depends on frequency and voltage. Generally, the G/ω shows a complex dependence as the increase of applied voltage for the Au/HfO_2/Si (*n*-type) sample, peaking near 0.5 V. The gate bias dependent peak shift of G/ω indicates that the surface potential responds to the gate bias when the Fermi level is located between the conduction band and midgap [30]. Similar peak shift of G/ω is also observed in the Au/HfO_2/Si (*p*-type) sample. Therefore, the interface states density could be calculated using the corrected $G/\omega - \mathrm{V}$ curve according to the following equation [31]:

$$D_{it} \approx \frac{2.5}{Aq}\left(\frac{G_P}{\omega}\right)_{\max} \tag{6}$$

where A and q are the electrode area (2.5×10^{-5} cm^2) and the element charge (1.60×10^{-19} C), respectively. The frequency dependent extracted interface state density is displayed in figure 2(e). Obviously, the interface state density monotonically increases as the increase of frequency for all samples, peaking at a fixed frequency. Then it monotonically decreases with the increase of frequency. The peak values of interface state density are 3.27×10^{12} eV^{-1}cm^{-2} for S1 sample ($f = 300$ kHz), 3.06×10^{12} eV^{-1}cm^{-2} for S4 sample ($f = 60$ kHz) and 1.87×10^{12} eV^{-1}cm^{-2} for S5 sample ($f = 40$ kHz), revealing that S5 sample holds a comparatively high interface quality between HfO_2 and Si.

Since the change of carrier occupancy only occurs when the energy of interface states is close to the Fermi level, the relative energy level (ΔE) of the interface states can be extracted. The distribution of interface state density below the conduction band, denoted as $E_C - E_T$ (location of the trap energy), can be determined according to the Shockley–Read–Hall statistics [32–34]:

$$\Delta E = E_C - E_T = k_B T \times \ln\left(\frac{\sigma v_{th} N_C}{\omega}\right) \tag{7}$$

where k_B, T, v_{th}, σ, N_C are the Boltzmann constant, the temperature, the thermal velocity of the majority carriers, the electron capture cross section of the trap state, and the effective density of state of the majority carrier in the conduction band, respectively. Figure 2(f) shows the exacted D_{it} as a function of the energy level for the typical S1 (n-type) and S4 (p-type). Clearly, the trap level E_T is close to the conduction band E_C for the n-type Si substrate while it is far from the E_C for the p-type Si substrate. The interface state density is larger ranging from 1.39×10^{12} $eV^{-1}cm^{-2}$ to 3.43×10^{12} $eV^{-1}cm^{-2}$ for n-type Si substrate ($\Delta E \in (0.22,\ 0.36)$) compared to that of p-type Si substrate range of 1.29×10^{11} $eV^{-1}cm^{-2}$ to 3.06×10^{12} $eV^{-1}cm^{-2}$ ($\Delta E \in (0.75,\ 0.9)$).

TD-SHG is an emerging effective method to reveal the semiconductor information, which is closely related to the electron excitation, transport and trapping/detrapping. When a high-energy pulsed laser irradiates on a typical oxide/semiconductor structure, the SHG signal rises rapidly indicating the creation of a time-dependent quasistatic electric field. This field originates from charge separation across the interface due to trapping of injected electrons while the holes remain in Si [35]. Additionally, the electrons could be significantly affected by the trapping density or interface state density. Correspondingly, the TD-SHG could be effectively used to estimate the defects and interface state density. The corresponding schematic of TD-SHG and the band structure are displayed in figures 3(a) and (b).

In the HfO_2 (15 nm)/Si system, the SHG signal originates from the trapped electrons relating to the interface state density and traps near the interface. In addition, the laser induced electron-hole separation could result in the electric field, which also contributes to the SHG signal. The signal of electric field induced SHG is closely linked to the dynamics of electron trapping/detrapping at the interface and it can be described by the solution of the equation [36]:

$$\frac{\mathrm{d}n_e}{\mathrm{d}t} = \left(n_{0e} - n_e\right)/\tau^e_{\mathrm{trap}} - n_e/\tau^e_{\mathrm{detrap}} \tag{8}$$

where n_{0e} and n_e are the initial quantity of unfilled electron trap concentration and filled electron trap concentration. $1/\tau^e_{\mathrm{trap}}$ and $1/\tau^e_{\mathrm{detrap}}$ denote the trapping rate due to the laser illumination and the detrapping rate. Given that the rate of $1/\tau^e_{\mathrm{trap}}$ is considerably high, the solution can be derived as:

$$n_e\left(t\right) = n_{0e} \cdot \left(1 - e^{-t/\tau^e_{\mathrm{trap}}}\right). \tag{9}$$

Hence, the following equation is used to describe the dynamics process of TD-SHG:

$$I^{2\omega}\left(t\right) = \left|a_0 + a_1\left(1 - e^{-t/\tau^e_{\mathrm{trap}}}\right)\right|^2 \tag{10}$$

here, a_0 and a_1 are the parameters closely associated with the initial value of SHG signal. The time constant τ is an effective indicator of the electron trapping rate. Figure 3(c) displays the time-dependent SHG signal under 200 mW over a time period of 5 s with P-in/P-out polarization (incidence angle at 45°).

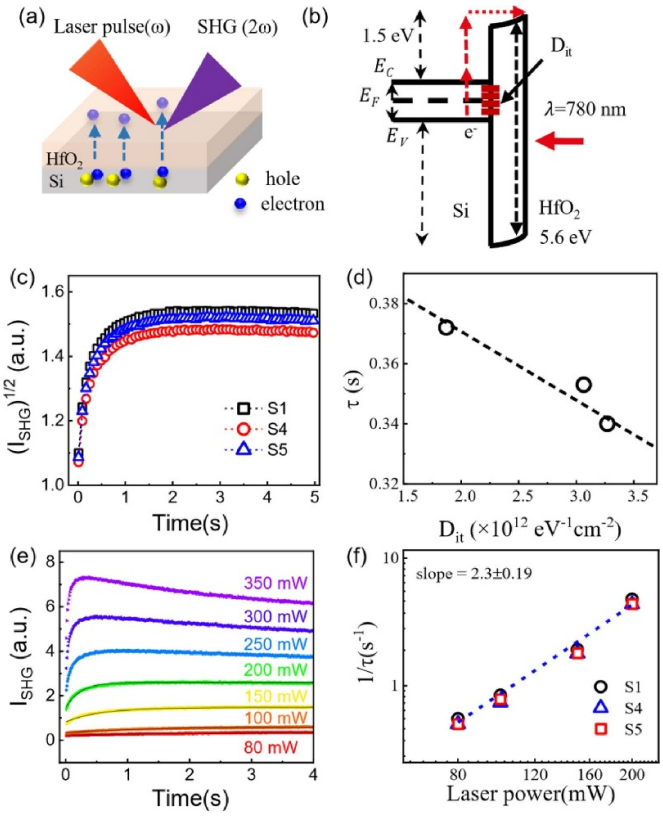

Figure 3. (a) Schematic diagram of second harmonic generation (SHG) for the HfO_2/Si sample. (b) Schematic energy band diagram for the laser induced electron excitation and transportation. (c) The time dependence of second harmonic generation (TD-SHG) for S1, S4 and S5. (d) The relationship between the interface states density and the extracted time constant from (c). (e) The TD-SHG of S5 under various laser power. (f) The laser power dependent of the extracted time constant for various samples in log scale. The solid line is the power law fitting.

The TD-SHG signal monotonically increase as the increase of time and it almost saturates after 2 s, which can be well fitted by the equation (10). The extracted time constants (τ) are 0.340, 0.353 and 0.372 s, for S1, S4 and S5 respectively. The TD-SHG corresponds to the interfacial electric field related to the laser induced electrons from Si valence band to the HfO_2 conduction band as well as the electron diffusion to the traps at the interface. The laser induced charge separation increases the interfacial electric field, namely $I^{2\omega}\left(t\right)$, up to a balanced interfacial electric field (saturation of SHG intensity). A linear relation between the extracted time constant τ and the interface state density is revealed (figure 3(d)), indicating that the TD-SHG is a sensitive and effective method for the characterization of semiconductor.

A typical laser power dependent TD-SHG for S5 sample is displayed in figure 3(e) with the laser power ranging from 80 to 350 mW. As for the laser power below 200 mW, the TD-SHG increases as the time followed by a saturation of SHG, which can be well fitted by a single exponential function (equation (10), solid fitting line in figure 3(e)). The extracted electron trapping rate due to the laser excitation follows

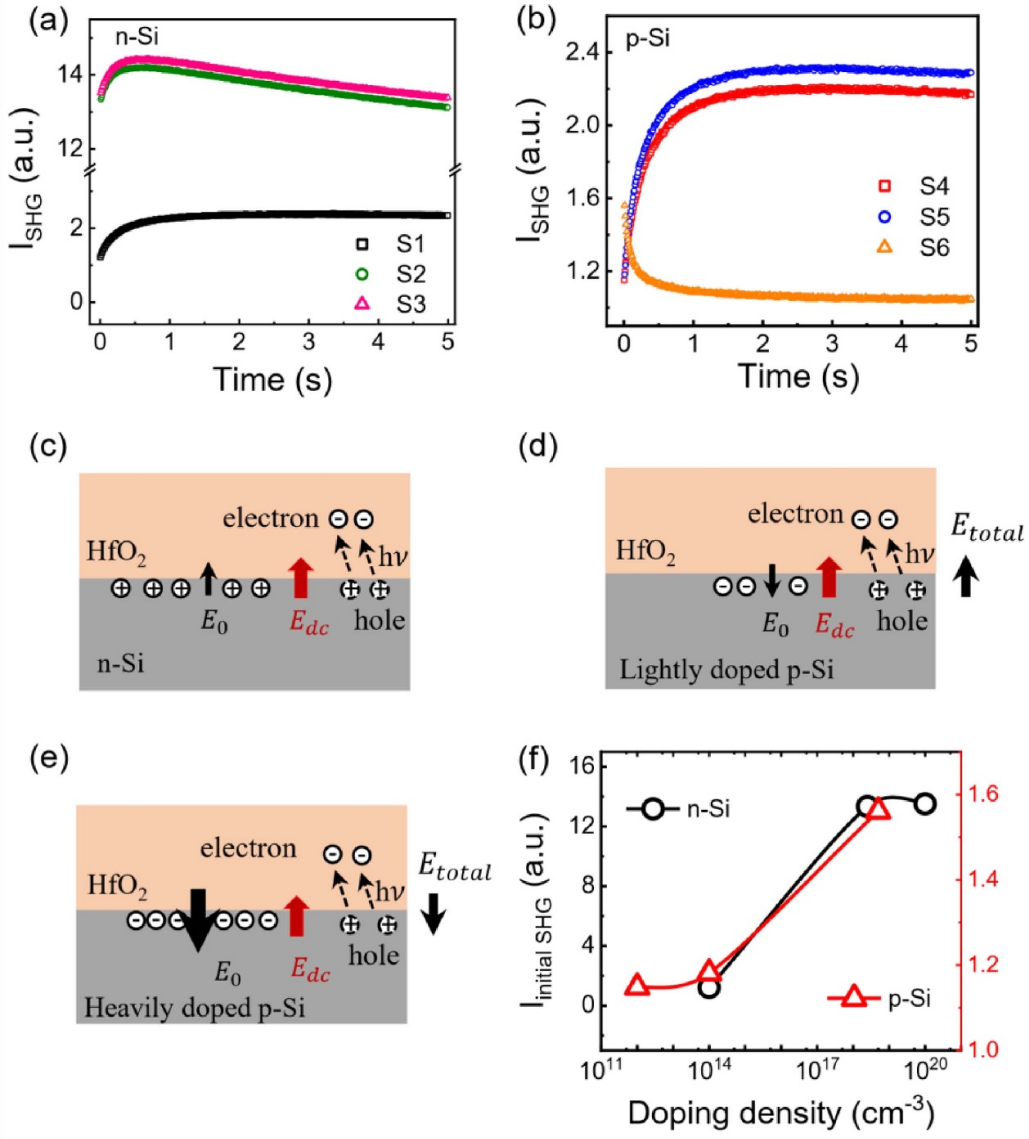

Figure 4. The TD-SHG of the HfO_2/Si samples with various dopant density for (a) *n*-type Si substrate and (b) *p*-type Si substrate. The schematic diagram of the interfacial electric field for (c) *n*-type Si substrate, (d) lightly doped *p*-Si substrate and (e) heavily doped *p*-Si substrate. (f) The dopant density dependent of initial SHG intensity.

a power law relation with the incident laser power, namely $1/\tau$ is proportional to $(I_\omega)^n$ $(1/\tau \propto (I_\omega)^n)$ [37]. The fitted parameter n is 2.3 (figure 3(f)), indicating that a two-photon absorption is required to promote electrons from the valence band of Si to the conduction band of HfO_2 at an incident photon energy of 1.59 eV. These results are consistent with the band structure depicted in figure 3(b), considering that the barrier height from the valence band of Si to conduction band of HfO_2 is 2.6 eV [38]. When the laser power is above 200 mW, the TD-SHG first rises in a short time, followed by a decayed SHG. The subsequent decay of SHG may be related to the delayed transfer of electrons from the oxide back to the Si substrate, which compensates the interfacial electric field [39]. In addition, the laser induced injection of holes into the oxide layer involving a four-photon process, which opposes the electron contributions. It could decrease the interfacial electric field, resulting the decay of SHG signal [40, 41].

The effect of dopant type/dopant density on the TD-SHG have been investigated to reveal the powerful ability of SHG to identify the defects/interface state density as well as the disclosing of substrate information (as shown in figure 4). The initial SHG signal and the dynamics of TD-SHG could be used to disclose the interfacial electric field due to the dopant type and dopant density of substrate. The density of the surface charge trapped at surface state Q_S increases with the dopant density (N) based on the relation $Q_S = \pm\sqrt{2\varepsilon_0\varepsilon_b |V_S| e_0 N}$, where ε_0, ε_b, e_0 and V_S are the vacuum permittivity, the dielectric constant of material, the elementary charge, and the band bending related to the dopant type and dopant density of substrate, respectively. Consequently, the interfacial electric field can be

estimated based on Q_S, which could be detected by the TD-SHG [42].

Clearly, the TD-SHG displays a similar trend in the HfO_2/Si (*n*-type) samples irrespective of the dopant density (figure 4(a)). Generally, the initial SHG signal increases as the raise of dopant density. At the low dopant density of Si substrate ($N_d \sim 10^{14}$ cm^{-3}) for the HfO_2/Si (*n*-type) sample, the TD-SHG measured at 200 mW laser irradiation monotonically increases as the evolution of time, which saturates at ∼1 s. Differently, the TD-SHG increases with the time at a short time range ($t < 0.5$ s), then it decays with the time for a long time period ($t > 0.5$ s) for the Si substrate with a high donor density ($N_d \geqslant 10^{17}$ cm^{-3}). As for the *n*-type Si substrate, the laser induced interfacial electric field is in the same direction of initial interfacial electric field, which could be used to explain the observed TD-SHG (figure 4(c)). The decay of SHG signal is likely to relate to the backflow of electrons, which cancels the laser induced interfacial electric field.

As for the HfO_2/Si (*p*-type) samples, the initial interfacial electric field points from the HfO_2 film towards the Si substrate crossing the interface. In the contrary, the laser induced interfacial electric field points to the HfO_2 film across the interface, which cancels the initial interfacial electric field, resulting the decrease of SHG signal. In fact, the TD-SHG is much complex compared to the simple model proposed above (figure 4(d)). The TD-SHG monotonically increases with the time and saturates after ∼1.5 s for the acceptor density below $\sim 10^{14}$ cm^{-3}. No decay process of SHG signal (no compensation) is observed due to the fast reverse of the interfacial electric field (opposite compared to initial interfacial electric field), which may be attributed to a quick compensation process (milliseconds) from a high-power laser irradiation as well as a small initial interfacial electric field (figure 4(d)). In order to testify the scenario, the TD-SHG of a high acceptor density of Si substrate ($N_a \sim 10^{18}$ cm^{-3}) with a large initial interfacial electric field is measured as shown in figure 4(b). The TD-SHG decreases as the time evolves, verifying that the total interfacial electric field (dominant field) is partially canceled by the laser induced interfacial electric field (figure 4(e)) [43]. The saturation of SHG signal is closely related to the balance of laser induced electron emission and electron-hole recombination, namely forming a stable interfacial electric field. Since the SHG can be used to resolved the interfacial electric field, the initial point of SHG signal ($t \sim 0$ s) should correspond to the initial electric field. Correspondingly, the initial SHG signal for various samples are shown in figure 4(f), which indicates that the SHG can be an effective way to estimate dopant density.

4. Conclusion

In conclusion, we employed the SHG technology to characterize the interfacial quality of HfO_2/Si structure. The connection is built between the interface state density extracted from traditional electrical method and SHG intensity from the fast SHG technology. We also report the measurement that a two-photon absorption is required to promote electrons from the valence band of Si to the conduction band of HfO_2 at an incident photon energy of 1.59 eV by detecting internal multiphoton light emission (IMPE) of SHG, which is inherently interface sensitive technique. Additionally, we quantified the sensitivity of initial second harmonic signals to doping concentration in both *p*-doped and *n*-doped HfO_2/Si systems at various doping concentrations. We attributed the variations in their TD-SHG shapes to the competitive effect of the electric field formed by the initial doping-induced charge traps and the photoexcited electrons. Our work contributes to utilizing efficient, non-destructive, non-contact optical second harmonic technique as a tool for diagnosing HfO_2/Si interface quality and evaluating substrate doping type and concentration. This provides potential research ideas and solutions for in-line, in-situ inspection in semiconductor fabrication lines.

Data availability statement

All data that support the findings of this study are included within the article (and any supplementary files).

Acknowledgments

This work was supported by the National Natural Science Foundation of China (Grant No. 12104005), the Scientific Research Foundation of the Higher Education Institutions for Distinguished Young Scholars in Anhui Province (Grant No. 2022AH020012), and the Innovation Project for Overseas Researcher in Anhui Province (Grant No. 2022LCX004). This work was also supported by Shanghai Aspiring Semiconductor Equipment Co., Ltd & Aspiring Semiconductor (Beijing) Co., Ltd We thank the micro- and nano-scale clean room at the AHU Quantum Materials Center for facilitating the experimental work. This work was also partially supported by the facilities at Center of Free Electron Laser & High Magnetic Field (FEL&HMF) in Anhui University.

CRediT authorship contribution statement

Li Ye: Investigation, Visualization, Formal analysis, Writing—original draft. **Libo Zhang:** Investigation, Visualization, Formal analysis. **Shaotong Wang:** Investigation. **Weiwei Zhao:** Resources, Investigation, Formal analysis. **Chongji Huang:** Investigation, Formal analysis. **Wenshuai Gao:** Investigation. **Xue Liu:** Investigation. **Tiaoyang Li:** Resources. **Tao Li:** Investigation. **Tai Min**: Investigation. **Mingliang Tian:** Conceptualization, Supervision, Writing—review & editing. **Xuegang Chen:** Conceptualization, Supervision, Formal analysis, Funding acquisition, Project administration, Writing—original draft, Writing—review & editing.

Conflict of interest

The authors have no conflicts to disclose.

ORCID iDs

Wenshuai Gao https://orcid.org/0000-0002-6174-974X
Tao Li https://orcid.org/0000-0002-3337-6202
Xuegang Chen https://orcid.org/0000-0002-3084-8681

References

[1] Chen A, Li C, Yao Q, Ma X, Li Y and Wang W 2022 Optimization of SiGe interface properties with ozone oxidation and a stacked HfO_2/Al_2O_3 dielectric for a SiGe channel FinFET transistor *Semicond. Sci. Technol.* **37** 125008
[2] Gieraltowska S, Wachnicki Ł, Witkowski B S, Godlewski M and Guziewicz E 2013 Properties of thin films of high-k oxides grown by atomic layer deposition at low temperature for electronic applications *Opt. Appl.* **43** 17–25
[3] Pokhriyal S, Biswas S and Prajapati R 2023 Structural, optical, and electrical properties of e-beam deposited metamaterials of granular CdSe thin films on glass substrates with a thin buffer layer of HfO_2 dielectric *Mater. Chem. Phys.* **294** 126950
[4] Robertson J and Wallace R M 2015 High-K materials and metal gates for CMOS applications *Mater. Sci. Eng.* R **88** 1–41
[5] He G, Zhu L, Liu M, Fang Q and Zhang L 2007 Optical and electrical properties of plasma-oxidation derived HfO_2 gate dielectric films *Appl. Surf. Sci.* **253** 3413–8
[6] Lu Y-H *et al* 2016 Effects of fabrication method on defects induced by nitrogen diffusion to the hafnium oxide layer in metal–oxide–semiconductor field effect transistors *Thin Solid Films* **620** 43–47
[7] Li Z, Feng Z, Xu Y, Feng Q, Zhu W, Chen D, Zhou H, Zhang J, Zhang C and Hao Y 2021 High performance β-Ga_2O_3 solar-blind metal–oxide–semiconductor field-effect phototransistor with hafnium oxide gate dielectric process *IEEE Electron Device Lett.* **42** 545–8
[8] He G, Zhu L, Sun Z, Wan Q and Zhang L 2011 Integrations and challenges of novel high-k gate stacks in advanced CMOS technology *Prog. Mater. Sci.* **56** 475–572
[9] Piscator J, Raeissi B and Engström O 2009 The conductance method in a bottom-up approach applied on hafnium oxide/silicon interfaces *Appl. Phys. Lett.* **94** 213507
[10] Bisi D, Chan S H, Liu X, Yeluri R, Keller S, Meneghini M, Meneghesso G, Zanoni E and Mishra U K 2016 On trapping mechanisms at oxide-traps in Al_2O_3/GaN metal-oxide-semiconductor capacitors *Appl. Phys. Lett.* **108** 112104
[11] Gielis J J H, Hoex B, van de Sanden M C M and Kessels W M M 2008 Negative charge and charging dynamics in Al_2O_3 films on Si characterized by second-harmonic generation *J. Appl. Phys.* **104** 073701
[12] Damianos D, Vitrant G, Lei M, Changala J, Kaminski-Cachopo A, Blanc-Pelissier D, Cristoloveanu S and Ionica I 2018 Second harmonic generation characterization of SOI wafers: impact of layer thickness and interface electric field *Solid-State Electron.* **143** 90–96
[13] Yen T-Y, Huang Y-H, Shih M-T, Chen W-T, Hung K-M and Lo K-Y 2023 Correlation of time-dependent nonlinear response with phosphorus concentration in Si ultrathin film *Surf. Interfaces* **36** 102541
[14] Yen T-Y, Shih M-T, Song L-F, Hung K-M and Lo K-Y 2023 Unveiling dopant concentration in boron doped Si ultrathin film: enhanced analysis using time-dependent second harmonic generation *Surf. Interfaces* **41** 103236
[15] Damianos D *et al* 2018 Field-effect passivation of Si by ALD-Al_2O_3: second harmonic generation monitoring and simulation *J. Appl. Phys.* **124** 125309
[16] Ionica I, Damianos D, Kaminski A, Vitrant G, Blanc-Pélissier D, Changala J, Kryger M, Barbos C and Cristoloveanu S 2016 Non-destructive characterization of dielectric—semiconductor interfaces by second harmonic generation *ECS Trans.* **72** 139–51
[17] Fomenko V, Gusev E P and Borguet E 2005 Optical second harmonic generation studies of ultrathin high-k dielectric stacks *J. Appl. Phys.* **97** 083711
[18] Mallick B, Saha D, Datta A and Ganguly S 2023 Noninvasive and contactless characterization of electronic properties at the semiconductor/dielectric interface using optical second-harmonic generation *ACS Appl. Mater. Interfaces* **15** 38888–900
[19] Vinod A, Rathore M S and Srinivasa Rao N 2018 Effects of annealing on quality and stoichiometry of HfO_2 thin films grown by RF magnetron sputtering *Vacuum* **155** 339–44
[20] Min D-H, Ryu T-H, Yoon S-J, Moon S-E and Yoon S-M 2020 Improvements in the synaptic operations of ferroelectric field-effect transistors using $Hf_{0.5}Zr_{0.5}O_2$ thin films controlled by oxygen partial pressures during the sputtering deposition process *J. Mater. Chem.* C **8** 7120–31
[21] Lee K, Park K, Lee H J, Song M S, Lee K C, Namkung J, Lee J H, Park J and Chae S C 2021 Enhanced ferroelectric switching speed of Si-doped HfO_2 thin film tailored by oxygen deficiency *Sci. Rep.* **11** 6290
[22] Chen X-Q, Xiong Y-H, Du J, Wei F, Zhao H-B, Zhang Q-Z, Zhang W-Q and Liang X-P 2017 Improving interfacial and electrical properties of $HfO_2/SiO_2/p$-Si stacks with N_2-plasma-treated SiO_2 interfacial layer *Rare Met.* **42** 2081–6
[23] Wang X, Zhang X, Xiong Y, Du J, Yang M and Wang L 2011 Fabrication and properties of Gd_2O_3-doped HfO_2 high k film by Co-sputtering *Rare Met.* **30** 647–50
[24] Zhao P, Khosravi A, Azcatl A, Bolshakov P, Mirabelli G, Caruso E, Hinkle C L, Hurley P K, Wallace R M and Young C D 2018 Evaluation of border traps and interface traps in HfO_2/MoS_2 gate stacks by capacitance–voltage analysis *2D Mater.* **5** 031002
[25] Xiao H and Huang S 2010 Frequency and voltage dependency of interface states and series resistance in Al/SiO_2/p-Si MOS structure *Mater. Sci. Semicond. Process.* **13** 395–9
[26] Tomer S, Kumar A, Devi M and Vandana 2023 ALD deposited bipolar HfOx films for silicon surface passivation *Surf. Interfaces* **41** 103208
[27] Lu W, Lu J X, Ou X, Liu X J, Cao Y Q, Li A D, Xu B, Xia Y D, Yin J and Liu Z G 2014 Determination of the density of the defect states in $Hf_{0.5}Zr_{0.5}O_2$ high-k film deposited by using rf-magnetron sputtering technique *AIP Adv.* **4** 087114
[28] Acar F Z, Buyukbas-Ulusan A and Tataroglu A 2018 Analysis of interface states in Au/ZnO/*p*-InP (MOS) structure *J. Mater. Sci., Mater. Electron.* **29** 12553–60
[29] Aktağ A, Mutale A and Yılmaz E 2020 Determination of frequency and voltage dependence of electrical properties of Al/($Er_2O_3/SiO_2/n$-Si)/Al MOS capacitor *J. Mater. Sci., Mater. Electron.* **31** 9044–51
[30] Hwang Y, Engel-Herbert R, Rudawski N G and Stemmer S 2010 Analysis of trap state densities at $HfO_2/In_{0.53}Ga_{0.47}As$ interfaces *Appl. Phys. Lett.* **96** 102910
[31] Zhu Z-F, Zhang H-Q, Liang H-W, Peng X-C, Zou J-J, Tang B and Du G-T 2017 Characterization of interface state density of Ni/*p*-GaN structures by capacitance/conductance

-voltage-frequency measurements *Chin. Phys. Lett.* **34** 097301
[32] Yoshioka H, Nakamura T and Kimoto T 2014 Characterization of very fast states in the vicinity of the conduction band edge at the SiO_2/SiC interface by low temperature conductance measurements *J. Appl. Phys.* **115** 014502
[33] Jia Y, Zeng K and Singisetti U 2017 Interface characterization of atomic layer deposited high-k on non-polar GaN *J. Appl. Phys.* **122** 154104
[34] Kim H, Yun H J, Choi S and Choi B J 2019 Interface trap characterization of AlN/GaN heterostructure with Al_2O_3, HfO_2, and HfO_2/Al_2O_3 dielectrics *J. Vac. Sci. Technol.* B **37** 041203
[35] Marka Z *et al* 2000 Characterization of x-ray radiation damage in Si/SiO_2 structures using second-harmonic generation *IEEE Trans. Nucl. Sci.* **47** 2256–61
[36] Marka Z, Pasternak R, Rashkeev S N, Jiang Y, Pantelides S T, Tolk N H, Roy P K and Kozub J 2003 Band offsets measured by internal photoemission-induced second-harmonic generation *Phys. Rev.* B **67** 045302
[37] Lei M, Yum J H, Banerjee S K, Bersuker G and Downer M C 2012 Band offsets of atomic layer deposited Al_2O_3 and HfO_2 on Si measured by linear and nonlinear internal photoemission *Phys. Status Solidi* b **249** 1160–5
[38] Melskens J, van de Loo B W H, Macco B, Black L E, Smit S and Kessels W M M 2018 Passivating contacts for crystalline silicon solar cells: from concepts and materials to prospects *IEEE J. Photovolt.* **8** 373–88
[39] Price J, An Y Q, Lysaght P S, Bersuker G and Downer M C 2009 Resonant photoionization of defects in $Si/SiO_2/HfO_2$ film stacks observed by second-harmonic generation *Appl. Phys. Lett.* **95** 052906
[40] Scheidt T, Rohwer E G, von Bergmann H M and Stafast H 2004 Charge-carrier dynamics and trap generation in native Si/SiO_2 interfaces probed by optical second-harmonic generation *Phys. Rev.* B **69** 165314
[41] Scheidt T, Rohwer E G, von Bergmann H M and Stafast H 2004 Optical second harmonic imaging: a versatile tool to investigate semiconductor surfaces and interfaces *Eur. Phys. J. Appl. Phys.* **27** 393–7
[42] Fiore J L, Fomenko V V, Bodlaki D and Borguet E 2011 Second harmonic generation probing of dopant type and density at the Si/SiO_2 interface *Appl. Phys. Lett.* **98** 041905
[43] Scheidt T, Rohwer E G, Neethling P, von Bergmann H M and Stafast H 2008 Ionization and shielding of interface states in native $p+$-Si/SiO_2 probed by electric field induced second harmonic generation *J. Appl. Phys.* **104** 083712